IEEE Access
Multidisciplinary | Rapid Review | Open Access Journal

Received May 15, 2018, accepted June 9, 2018, date of publication June 13, 2018, date of current version July 12, 2018.

*Digital Object Identifier 10.1109/ACCESS.2018.2846770*

# Model Predictive Virtual Flux Control to Improve Performance Under Distorted Input Voltage Conditions

**JAE-CHANG KIM AND SANGSHIN KWAK, (Member, IEEE)**
School of Electrical and Electronics Engineering, Chung-Ang University, Seoul 156-756, South Korea

Corresponding author: Sangshin Kwak (sskwak@cau.ac.kr)

This work was supported by the National Research Foundation of Korea through the Korean Government (MSIP) under Grant 2017R1A2B4011444.

**ABSTRACT** This paper proposes a model predictive virtual flux control (MPVFC) method that can mitigate the degradation of the total harmonic distortion of rectifier input currents experienced by active front-end (AFE) rectifiers when input voltages are distorted by harmonics. The proposed method utilizes a cost function based on virtual fluxes, which are robust to input voltage distortions, to control the rectifiers. For the calculation of the proposed cost function which consists of a predictive value of the rectifier virtual flux and a reference of the rectifier virtual flux, the dynamics of AFE rectifiers and the definition of the integration in the discrete time domain are used. Also, the phase of the reference current which is needed when calculating the reference of the rectifier virtual flux is obtained by the input virtual flux. The proposed MPVFC method shows better input current waveforms with lower total harmonic distortion than those obtained with the conventional model predictive control method under input voltage distortion conditions, which was proved via simulations and experiments.

**INDEX TERMS** Active front-end (AFE) rectifier, model predictive control, virtual flux.

## I. INTRODUCTION

Active front-end (AFE) rectifiers have been widely utilized because of their low total harmonic distortion (THD) of the input current, adjustable output voltage, unity power factor operation, and regenerative capability [1]. For a control of AFE rectifiers, various control algorithms such as the voltage-oriented control (VOC), the direct power control (DPC), the direct torque control (DTC), the fuzzy-logic control, and the sliding mode nonlinear control have been proposed [2]–[9]. Among them, the VOC and the DPC methods are considered as general control methods for AFE rectifiers. Although these algorithms can yield superior performance under normal input voltage conditions, they face performance deterioration of the AFE rectifier when harmonic components are included in the input voltage, due to their operating principle involving the use of the input voltage itself. Virtual flux-based control methods have been developed to overcome this drawback [10], [11]. Virtual flux-based control schemes are simple to implement and have the advantage of filtering the harmonic components of the input voltages. In recent years, model predictive control (MPC) methods, which have intuitive, effective, and good dynamic characteristics, have been developed thanks to the rapid development of cost-effective microprocessors [13], [14]. For AFE rectifier control, the model predictive current control (MPCC) and the model predictive direct power control (MPDPC) methods have been proposed [15]–[23], [26]–[29]. The MPCC algorithms directly control the input current of the rectifier by using the input current as a control variable, whereas the MPDPC methods directly adjust the input power of the rectifier based on the input power as a control target. Although those methods can successfully control the AFE rectifier with accurate output voltage regulation and with unity power factor, performance of these algorithms is deteriorated by input voltage distortion. To alleviate adverse effects of harmonic distortion of the input voltage on the rectifier control, MPDPC methods based on virtual fluxes (VF-MPDPC) have been proposed [24], [25]. In the VF-MPDPC methods, the cost function for the AFE rectifier control is calculated by virtual fluxes instead of the input voltage. Due to the cost function obtained by the virtual fluxes, the VF-MPDPC methods can mitigate the performance reduction caused by the input voltage distortion. Although the VF-MPDPC methods can greatly improve the

AFE control performance under distorted input voltages, these control methods are restricted to power control because they are based on the direct power control methods. A purpose of this paper is to develop the AFE control method based on the model predictive control method rather than power control methods, which is robust to input voltage distortion.

This paper proposes a model predictive virtual flux control (MPVFC) method that can mitigate the degradation of the total harmonic distortion of rectifier input currents experienced by active front-end (AFE) rectifiers when input voltages are distorted by harmonics. The proposed method utilizes a cost function based on virtual fluxes, which are robust to input voltage distortions, to control the rectifiers. For the calculation of the proposed cost function which consists of a predictive value of the rectifier virtual flux and a reference of the rectifier virtual flux, the dynamics of AFE rectifiersand the definition of the integration in the discrete time domain are used. Also, the phase of the reference current which is needed when calculating the reference of the rectifier virtual flux is obtained by the input virtual flux. The proposed MPVFC method shows better input current waveforms with lower total harmonic distortion than those obtained with the conventional model predictive control method under input voltage distortion conditions, which was proved via simulations and experiments.

## II. CONVENTIONAL METHOD: MODEL PREDICTIVE CURRENT CONTROL METHOD

Fig. 1 shows a general AFE rectifier. In Fig. 1, $v_{sa}$ is the $a$-phase input voltage, $R$ is a line resistance, $L$ is a line inductance, $i_{cona}$ is the $a$-phase rectifier input current, and $V_{dc}$ is the output voltage of the rectifier. In addition, $S_a$, $S_b$, and $S_c$ represent the upper switches at the $a$-phase, $b$-phase, and $c$-phase, respectively. Furthermore, $\bar{S}_a$, $\bar{S}_b$, and $\bar{S}_c$ denote the lower switches at the $a$-phase, $b$-phase, and $c$-phase respectively. The upper and lower switches connected at the same phase operate complementarily. Fig. 2 shows a block diagram of the general control method for AFE rectifiers. The conventional MPCC and MPDPC methods, as well as the MPVFC method proposed in this paper, are based on the block diagram shown in Fig. 2, in which the control block is designed differently according to specific control algorithms using different control targets. In the case of the MPCC method, the rectifier input currents

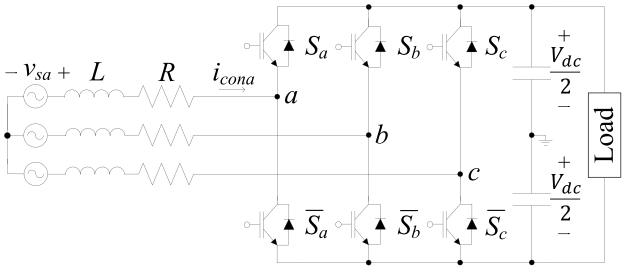


**FIGURE 1.** Active front-end (AFE) rectifier.

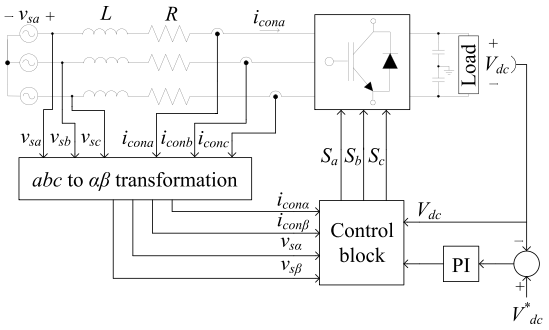


**FIGURE 2.** Block diagram of the AFE rectifier.

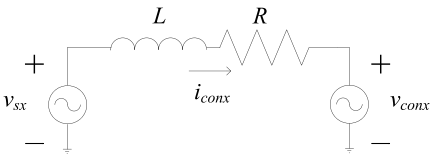


**FIGURE 3.** Simplified per-phase equivalent of the circuit of Fig. 1.

are predicted based on the rectifier dynamic equations and the measured signals in order to force the rectifier input currents to track the reference currents. Fig. 3 represents a simplified per-phase equivalent circuit of the one in Fig. 1, where, $v_{conx}(x = a, b, \text{and } c)$ is the rectifier input voltage at each phase. The dynamic equations in the continuous time domain are obtained from Fig. 3 as shown in (1),

$$v_{sx}(t) = L\frac{di_{conx}(t)}{dt} + Ri_{conx}(t) + v_{conx}(t), \tag{1}$$

where, $x = a, b,$ and $c$. The dynamic equations in the discrete time domain can be derived via Euler approximations, as shown in (2).

$$v_{sx}(k) = L\frac{i_{conx}(k+1) - i_{conx}(k)}{T_s} + Ri_{conx}(k) + v_{conx}(k). \tag{2}$$

In (2), $v_{sx}(k)$ is the $k^{\text{th}}$ input voltage, $i_{conx}(k+1)$ is the $(k+1)^{\text{th}}$ rectifier input current, $i_{conx}(k)$ is the $k^{\text{th}}$ rectifier input current, $T_s$ is the sampling period, and $v_{conx}(k)$ represents the $k^{\text{th}}$ rectifier input voltage in the $abc$ frame. From (2), the $(k+1)^{\text{th}}$ predictive rectifier input current vector in the $\alpha\beta$ frame $\mathbf{i}_{con}(k+1) = [i_{con\alpha}(k+1)\ i_{con\beta}(k+1)]^T$ is obtained as shown in (3). The $abc$ to $\alpha\beta$ frame conversion of the three-phase current used to derive the predictive rectifier current vector in (3) is represented by the matrix in (4). The three-phase voltage is also converted in the same way.

$$\mathbf{i}_{con}(k+1) = \left(1 - \frac{RT_s}{L}\right)\mathbf{i}_{con}(k) + \frac{T_s}{L}(\mathbf{v}_s(k) - \mathbf{v}_{con}(k)). \tag{3}$$

$$\begin{bmatrix} i_\alpha \\ i_\beta \end{bmatrix} = \frac{2}{3}\begin{bmatrix} 1 & -\frac{1}{2} & -\frac{1}{2} \\ 0 & \frac{\sqrt{3}}{2} & -\frac{\sqrt{3}}{2} \end{bmatrix}\begin{bmatrix} i_a \\ i_b \\ i_c \end{bmatrix}. \tag{4}$$

In (3), $\mathbf{v}_s(k) = [v_{s\alpha}(k)\, v_{s\beta}(k)]^T$ represents the $k^{\text{th}}$ input voltage vector in the $\alpha\beta$ frame. In addition, $\mathbf{v}_{con}(k) = [v_{con\alpha}(k)\, v_{con\beta}(k)]^T$ is the $k^{\text{th}}$ rectifier input voltage vector of the $\alpha\beta$ frame, which is determined by the switching states of the AFE rectifier. The rectifier input voltages in the $\alpha\beta$ frame, according to the switching states, are summarized in Table 1.

**TABLE 1. Rectifier input voltage corresponding to the switching states.**

| $v_{con\alpha}$ | $v_{con\beta}$ | $S_a$ | $S_b$ | $S_c$ |
|---|---|---|---|---|
| 0 | 0 | 0 | 0 | 0 |
| $(2/3)V_{dc}$ | 0 | 1 | 0 | 0 |
| $(1/3)V_{dc}$ | $(\sqrt{3}/3)V_{dc}$ | 1 | 1 | 0 |
| $-(1/3)V_{dc}$ | $(\sqrt{3}/3)V_{dc}$ | 0 | 1 | 0 |
| $-(2/3)V_{dc}$ | 0 | 0 | 1 | 1 |
| $-(1/3)V_{dc}$ | $-(\sqrt{3}/3)V_{dc}$ | 0 | 0 | 1 |
| $(1/3)V_{dc}$ | $-(\sqrt{3}/3)V_{dc}$ | 1 | 0 | 1 |
| 0 | 0 | 1 | 1 | 1 |

As can be seen from (3), the $(k+1)^{\text{th}}$ predictive rectifier input current vector changes depending on the switching state of the rectifier. Using this property, an optimal switching state that produces the predictive rectifier input current vector closest to the reference vector $\mathbf{i}^*_{con}(k+1) = [i^*_{con\alpha}(k+1)\, i^*_{con\beta}(k+1)]^T$ is used for the rectifier control at the $(k+1)^{\text{th}}$step. The reference current vector can be obtained using the output of the PI controller of the output voltage of the AFE rectifier and the input voltage phase for the unity power factor operation. A cost function as described in (5) is used to control the AFE rectifier so that the predictive rectifier input current vector obtained above tracks the reference of the rectifier input current vector. The switching state that minimizes the cost function presented in (5) is selected as the optimal switching state.

$$g = \left|\mathbf{i}^*_{con}(k+1) - \mathbf{i}_{con}(k+1)\right|. \tag{5}$$

Fig. 4 represents the MPCC control block. Because the MPCC method directly uses the input voltage for the AFE rectifier control, the AFE rectifier performance obtained by the MPCC method can be degraded if the input voltage is distorted. In the proposed MPVFC method, the virtual flux, which is resistant to the distorted input voltage, is used as a control variable, and thus, the proposed method is more effective against distortions of the input voltage than the MPCC method.

## III. PROPOSED METHOD: MODEL PREDICTIVE VIRTUAL FLUX CONTROL METHOD

The introduction of virtual flux started with the idea that the input voltage, the line resistance, and the line inductance of an AFE rectifier can be regarded as a virtual ac motor. The value obtained by integrating the line to line voltage of the virtual ac motor is called the virtual flux. By extending this concept, a value obtained by integrating a physical voltage is called a virtual flux. The integration has characteristics of the low-pass filter [10], [11], [24], [25], [30]. Therefore, controlling

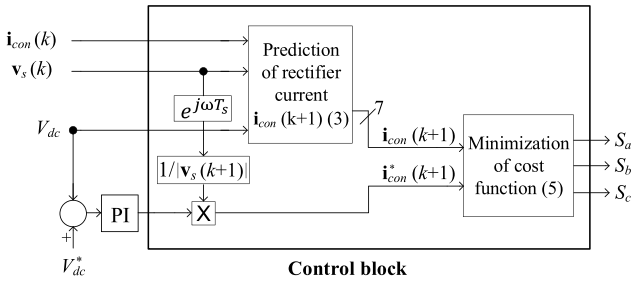


**FIGURE 4. Control block for the model predictive current control scheme.**

the AFE rectifier using the virtual flux can mitigate the performance degradation of the rectifier because of the filtering effects on the harmonic components present in distorted input voltages.

The proposed MPVFC method uses the virtual flux of the rectifier input voltage as a control variable to control the AFE rectifier. In order to design the model predictive control method utilizing the virtual flux, dynamic equations based on the virtual flux are derived in this paper. By integrating both sides of the dynamic equations shown in (1), the dynamic equations based on the virtual flux can be obtained as shown in (6),

$$\psi_{sx}(t) = Li_{conx}(t) + \int Ri_{conx}(t)\, dt + \psi_{conx}(t), \tag{6}$$

where, $x = a$, $b$, and $c$. In addition, $\psi_{sx}(t)$ represents the virtual flux of the input voltage and $\psi_{conx}(t)$ represents the virtual flux of the rectifier input voltage in the $abc$ frame. Using the $abc$ to $\alpha\beta$ frame conversion, the virtual flux-based dynamic equation in the discrete time domain and the $\alpha\beta$ frame is obtained as shown in (7). In that equation, $\boldsymbol{\psi}_s(k) = [\psi_{s\alpha}(k)\, \psi_{s\beta}(k)]^T$ is the $\text{k}^{\text{th}}$ input virtual flux vector and $\boldsymbol{\psi}_{con}(k) = [\psi_{con\alpha}(k)\, \psi_{con\beta}(k)]^T$ represents the $k^{\text{th}}$ rectifier virtual flux vector in the $\alpha\beta$ frame.

$$\boldsymbol{\psi}_s(k) = L\mathbf{i}_{con}(k) + \sum\nolimits_{n=0}^{n=k} R\mathbf{i}_{con}(n)\, T_s + \boldsymbol{\psi}_{con}(k). \tag{7}$$

By shifting (7) one step ahead, the future reference vector of the rectifier virtual flux at the $(k+1)^{\text{th}}$ instant, $\boldsymbol{\psi}^*_{con}(k+1) = \left[\psi^*_{con\alpha}(k+1)\, \psi^*_{con\beta}(k+1)\right]^T$ can be obtained as

$$\boldsymbol{\psi}^*_{con}(k+1) = \boldsymbol{\psi}_s(k+1) - L\mathbf{i}^*_{con}(k+1) - \sum\nolimits_{n=0}^{n=k+1} R\mathbf{i}^*_{con}(n)\, T_s, \tag{8}$$

where, $\boldsymbol{\psi}_s(k+1) = [\psi_{s\alpha}(k+1)\, \psi_{s\beta}(k+1)]^T$ is the $(k+1)^{\text{th}}$ virtual flux vector of the input voltage in the $\alpha\beta$ frame. The future virtual flux vector of the input voltage at the $(k+1)^{\text{th}}$ instant $\boldsymbol{\psi}_s(k+1)$ can be obtained by integrating the input voltage vector in the discrete time domain as

$$\boldsymbol{\psi}_s(k+1) = \sum\nolimits_{n=0}^{n=k} \mathbf{v}_s(n)\, T_s + \mathbf{v}_s(k+1)T_s, \tag{9}$$

where, $\mathbf{v}_s(k+1) = [v_{s\alpha}(k+1)\, v_{s\beta}(k+1)]^T$ is the input voltage vector in the $\alpha\beta$ frame at the $(k+1)^{\text{th}}$ instant.

The $(k+1)^{\text{th}}$ input voltage vector required to calculate the $(k+1)^{\text{th}}$ input virtual flux vector shown in (9) can be obtained, using the measured $k^{\text{th}}$ input voltage vector, using the following equation:

$$\mathbf{v}_s(k+1) = \mathbf{v}_s(k)e^{j\omega T_s}. \tag{10}$$

The future reference input current vector at the $(k+1)^{\text{th}}$ step $\mathbf{i}^*_{con}(k+1)$ which is required for (8), can be obtained with the PI controller for the rectifier output voltage and the virtual flux vector of the input voltage. The magnitude of the reference current vector is obtained using the output of the PI controller, whereas the phase of the reference current vector is determined by the virtual flux vector of the input voltage. Fig. 5 shows the input voltage vector and the virtual flux vector of the input voltage in the $\alpha\beta$ axis. As shown in the figure, to make the input voltage and the rectifier input current be in phase for the unity power factor, the $\alpha$ component of the reference input current vector should have a 180ř phase difference with the $\beta$ component of the virtual flux vector of the input voltage $\psi_{s\beta}$. In addition, the $\beta$ component of the reference input current vector should be in phase with the $\alpha$ component of the virtual flux vector of the input voltage $\psi_{s\alpha}$. Based on the future virtual flux vector of the input voltage and the construction of the future reference current vector, the future reference virtual flux vector of the rectifier input voltage can be obtained using (8). The future virtual flux vector of the rectifier input voltage at the $(k+1)^{\text{th}}$ step can be written as

$$\boldsymbol{\psi}_{con}(k+1) = \sum_{n=0}^{n=k} \mathbf{v}_{con}(n)\,T_s + \mathbf{v}_{con}(k+1)\,T_s, \tag{11}$$

where, $\mathbf{v}_{con}(k+1) = \left[v_{con\alpha}(k+1)\, v_{con\beta}(k+1)\right]^T$ is the rectifier input voltage vector at the $n^{\text{th}}$ and $(k+1)^{\text{th}}$ step in the $\alpha\beta$ frame. Based on the definition of the virtual flux and (7), the future virtual flux vector of the rectifier input voltage at the $(k+1)^{\text{th}}$ step in (11) can be derived as shown in (12). It can be seen from the last term in (12) that the future virtual flux vector of the rectifier input voltage depends on the future rectifier input voltage vector $\mathbf{v}_{con}(k+1)$, which changes with the switching states of the AFE rectifier. Therefore, seven possible values for the future virtual flux vector of the rectifier input voltage, which are obtained by considering all switching states of the rectifier except the redundant switching state, are predicted according to the seven rectifier input voltage vectors using (12).

$$\boldsymbol{\psi}_{con}(k+1) = \boldsymbol{\psi}_s(k) - L\mathbf{i}_{con}(k) - \sum_{n=0}^{n=k} R\mathbf{i}_{con}(n)\,T_s + \mathbf{v}_{con}(k+1)\,T_s. \tag{12}$$

The seven predicted values of the future virtual flux vectors of the rectifier input voltage in (12) can be compared with the reference value of the future virtual flux vector of the rectifier input voltage in (8) to select the optimal value for the rectifier input voltage vector, leading to the optimal switching state. In practical control methods realized with microprocessors, which have inevitable delay effects, the proposed MPVFC method for AFE rectifiers is constructed with a delay compensation algorithm using the cost function at the $(k+2)^{\text{th}}$ instant [17]. As a result, the two-step future virtual flux vector of the rectifier input voltage, shifted one step ahead, is obtained by

$$\boldsymbol{\psi}_{con}(k+2) = \boldsymbol{\psi}_s(k+1) - L\mathbf{i}_{con}(k+1) - \sum_{n=0}^{n=k+1} R\mathbf{i}_{con}(n)\,T_s + \mathbf{v}_{con}(k+2)\,T_s, \tag{13}$$

where, $\boldsymbol{\psi}_{con}(k+2) = [\psi_{con\alpha}(k+2)\ \psi_{con\beta}(k+2)]^T$ denotes the two-step future rectifier virtual flux vector. The one-step future virtual flux vector of the input voltage $\boldsymbol{\psi}_s(k+1)$ and the one-step future rectifier input current vector $\mathbf{i}_{con}(k+1)$ can be obtained using (9) and (3). Likewise, the one-step future reference virtual flux vector of the rectifier input voltage in (8) is shifted one step ahead to obtain the reference vector at the $(k+2)^{\text{th}}$ instant. Based on the two-step future values of the virtual flux vectors, the cost function is determined as

$$g_{flux} = \left|\boldsymbol{\psi}^*_{con}(k+2) - \boldsymbol{\psi}_{con}(k+2)\right|. \tag{14}$$

Fig. 6 shows the control block diagram of the proposed MPVFC method utilizing the virtual flux vectors as control variables. Due to the use of the virtual flux vectors, proposed method can yield improved performance under input voltage distortions, in comparison with the MPCC method which uses the rectifier input currents as control variables. To remove unwanted dc components associated with the integration, the actual rectifier control based on the virtual flux utilizes a low-pass filter instead of integrating the voltage for obtaining the virtual flux [12]. Fig. 7 shows Bode diagrams of the integrator and the low-pass filter. From Fig. 7, it can be seen that compensations are needed to realize the desired integrator based on the low-pass filter. This compensation is called the compensation gain $C$ and is expressed as shown in (15) where $\omega_c$ and $f$ means the cut-off frequency of the low-pass filter and the fundamental frequency of the input voltage, respectively. Table 2 shows relationships of the integrator, the low-pass filter, and the compensation gain $C$ in the frequency domain and the fundamental frequency. The magnitude and the phase of the compensation gain is $\sqrt{(2\pi f)^2+\omega_c^2}/(2\pi f)$ and $-\arctan(\omega_c/(2\pi f))$, respectively. Therefore, the required

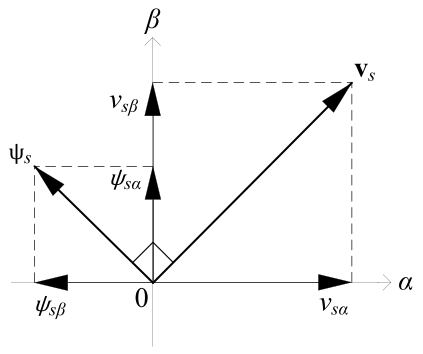


**FIGURE 5.** Input voltage vectors and virtual flux vectors of the input voltage in the $\alpha\beta$ axis.

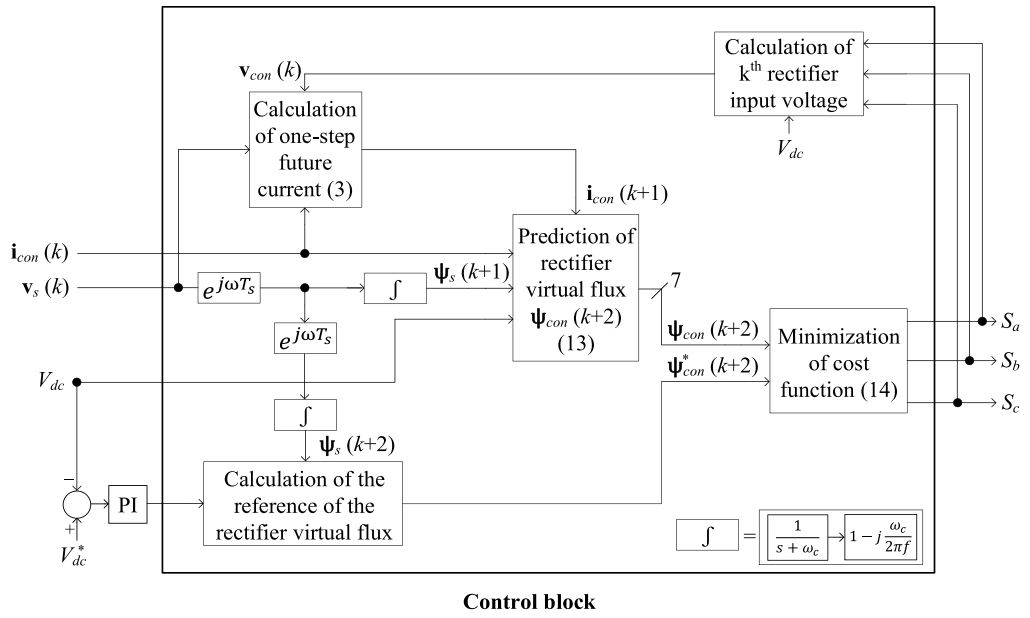


**FIGURE 6.** Control block diagram of the proposed MPVFC method.

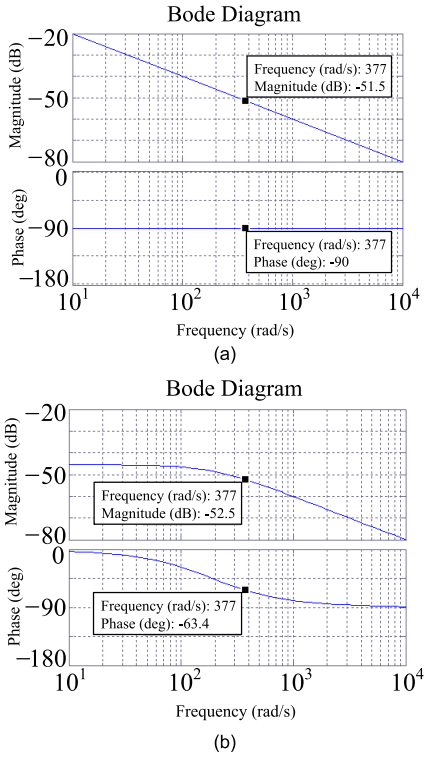


**FIGURE 7.** Bode diagram of (a) the integrator and (b) the low-pass filter with the cut-off frequency of $\omega_c = 188.5$ (rad/s).

integration can be realized using the low-pass filter and the compensation gain $C$ in the fundamental frequency of the input voltage. The cut-off frequency $\omega_c$ is usually set from 10 % to 50 % of the angular frequency of the input voltage [12]. Fig. 8 shows the block diagram of the virtual

**TABLE 2.** Relationship of the integrator, the low-pass filter, and the compensation gain $C$ in the frequency domain and the fundamental frequency $f$.

| | Integrator | Low-pass filter | Compensation gain $C$ |
|---|---|---|---|
| **Expression** | $\frac{1}{j(2\pi f)}$ | $\frac{1}{j(2\pi f)+\omega_c}$ | $1-j\frac{\omega_c}{2\pi f}$ |
| **Magnitude** | $\frac{1}{2\pi f}$ | $\frac{1}{\sqrt{(2\pi f)^2+\omega_c^2}}$ | $\frac{\sqrt{(2\pi f)^2+\omega_c^2}}{2\pi f}$ |
| **Phase** | $-\frac{\pi}{2}$ | $-\arctan(\frac{2\pi f}{\omega_c})$ | $-\arctan(\frac{\omega_c}{2\pi f})$ |

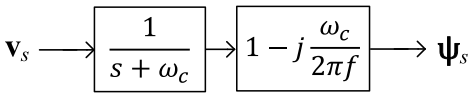


**FIGURE 8.** Calculation of the virtual flux using the low-pass filter and compensation gain.

flux calculation method using the low-pass filter and the compensation gain.

$$C = 1 - j\frac{\omega_c}{2\pi f}. \tag{15}$$

## IV. SIMULATION RESULTS

Simulations with the parameters shown in Table 3 were conducted to verify the performance of the proposed MPVFC method. In addition, the simulation results obtained with both the proposed MPVFC method using the virtual flux vectors and the conventional MPCC method based on the rectifier input current vectors were compared under the

**TABLE 3. Parameters for simulation.**

| Parameter | Value |
|---|---|
| Sampling period $T_s$ | 50 $\mu$s |
| Input phase voltage $v_s$ | 220 $V_{rms}$ |
| Line inductance $L$ | 10 mH |
| Line resistance $R$ | 1 Ω |
| Input voltage frequency $f$ | 60 Hz |
| Output capacitance $C$ | 550 $\mu$F |
| Load resistance $R_{out}$ | 100 Ω |
| Output voltage reference $V_{dc}^*$ | 650 V |

same conditions and parameters. Figs. 9 (a) and (b) show the steady-state simulation results of the MPCC and the MPVFC methods in the case in which the input voltage source has no distortion, respectively. It can be seen that the output voltages generated by both methods track the reference voltage of 650 V. Furthermore, we confirmed that the three-phase rectifier input currents of the two methods were balanced and had a sinusoidal waveform in phase with the input voltage, leading to the unity power factor.

The three-phase input voltage source distorted with the fifth harmonic components can be written as

$$\begin{aligned} v_{sa} &= V_{amp}\cos(\omega t)+\mu_a V_{amp}\cos(5\omega t) \\ v_{sb} &= V_{amp}\cos\left(\omega t-\frac{2}{3}\pi\right)+\mu_b V_{amp}\cos(5\omega t+\frac{2}{3}\pi) \\ v_{sc} &= V_{amp}\cos\left(\omega t+\frac{2}{3}\pi\right)+\mu_c V_{amp}\cos(5\omega t-\frac{2}{3}\pi), \quad (16) \end{aligned}$$

where, $V_{amp}$ represents the magnitude of the fundamental component of the input voltages and $\mu_i (i = a, b, c)$ is a factor of the magnitude of the fifth harmonic component to the magnitude of the fundamental component for each phase of the input voltage. Figs. 10 (a) and (b) represent the simulation results of the MPCC and the MPVFC methods, respectively, for the case in which only the $a$-phase input voltage contains the fifth harmonic component, i.e., $\mu_a = 0.1$ and $\mu_b = \mu_c = 0$. It can be seen in Fig. 10 (a) that the rectifier input currents produced by the conventional MPCC method are distorted when the input voltage is distorted by harmonics. On the other hand, the proposed MPVFC method, as shown in Fig. 10 (b), generates rectifier input currents that are less contaminated than those of the conventional MPCC method, despite the distortion of the input voltage. It can also be seen that the output voltage in both methods follows the reference of 650 V under $a$-phase distortion. Therefore, the proposed MPVFC method can mitigate the performance degradation of the AFE rectifier despite the presence of input voltage distortions, compared with the MPCC method.

Fig. 11 shows the simulation results when the three-phase input voltages are exposed to balanced distortion with fifth harmonic components, i.e., $\mu_a = \mu_b = \mu_c = 0.1$ in (16). Because of the distortion in the three-phase input voltages with the fifth harmonic components, the rectifier input current waveforms of the conventional

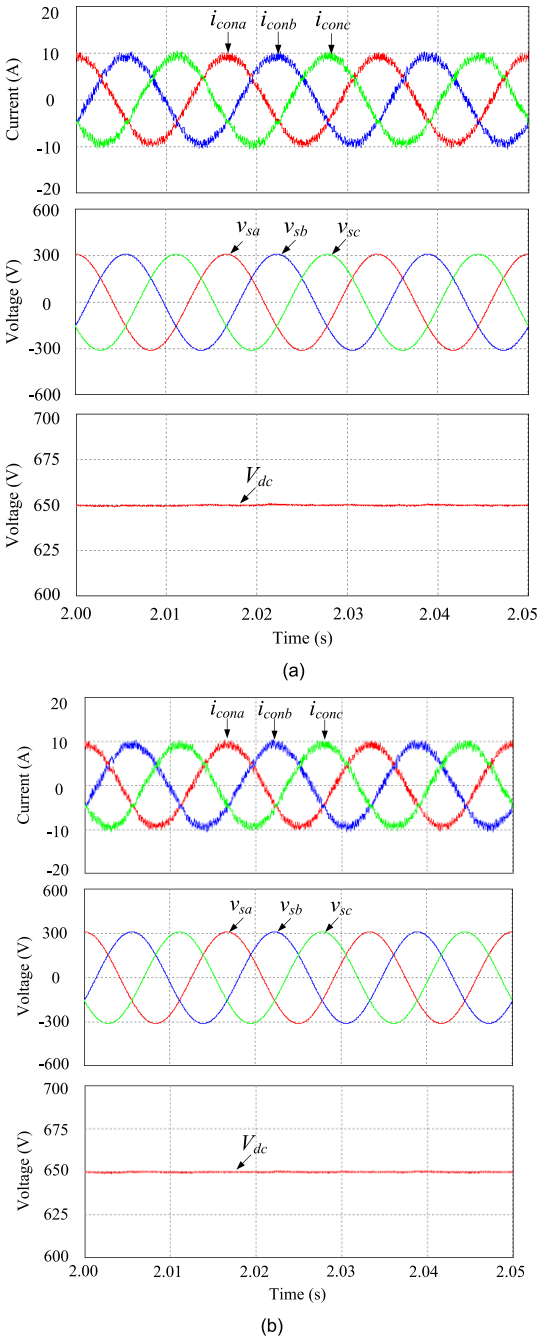


**FIGURE 9. Simulation results of the three-phase rectifier input currents, the three-phase input voltages with no distortion, and the output dc voltage in the steady state obtained with (a) the conventional MPCC method and (b) the proposed MPVFC method.**

MPCC method, shown in in Fig. 11 (a), are worse than those for the distortion of only the $a$-phase input voltage, shown in Fig. 10 (a). However, as shown in Fig. 11 (b), the proposed MPVFC method, despite the distortion of the three-phase input voltages, can produce sinusoidal input currents with less distortion than the conventional MPCC method. As shown in Figs. 11 (a) and (b), the output voltage of both methods tracks the reference of 650 V under three-phase distortion of the input voltage.

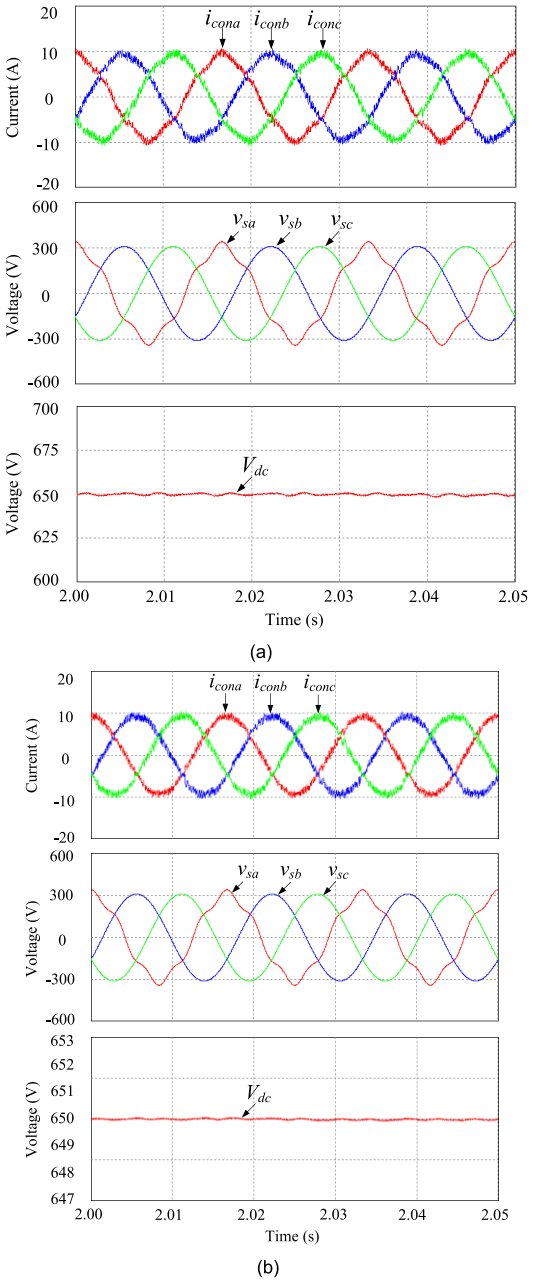


**FIGURE 10.** Simulation results of the three-phase rectifier input currents, the three-phase input voltages with *a*-phase distortion ($\mu_a = 0.1$), and the output dc voltage in the steady state obtained by (a) the conventional MPCC method and (b) the proposed MPVFC method.

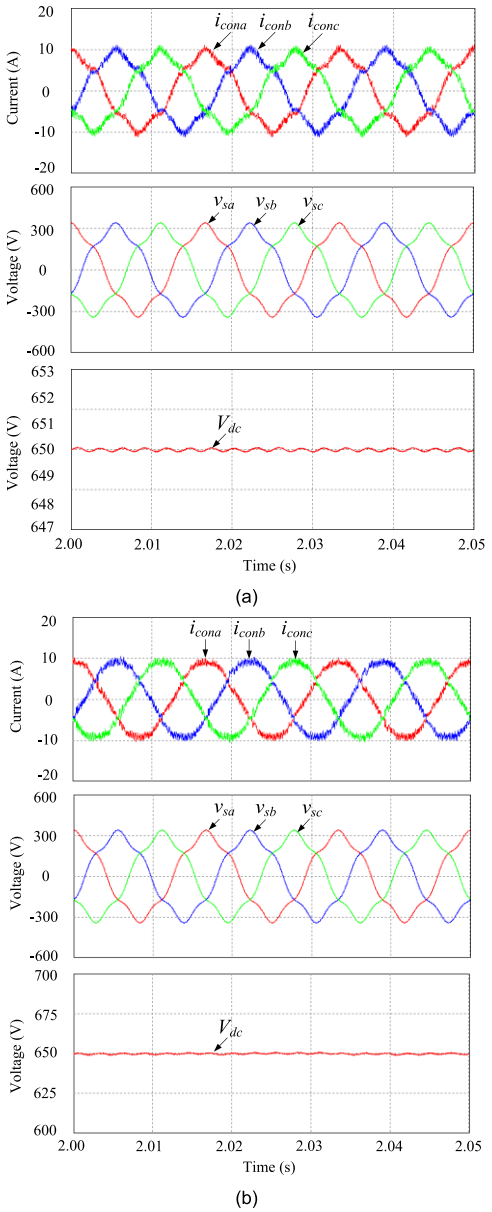


**FIGURE 11.** Simulation results of the three-phase rectifier input currents, the three-phase input voltages, and the output *dc voltage for* balanced distortion with fifth harmonics in the input voltages ($\mu_a = \mu_b = \mu_c = 0.1$) obtained by (a) the conventional MPCC method and (b) the proposed MPVFC method.

Fig. 12 shows the simulation results when the periodical change of the output reference voltage $V_{dc}^*$ and the output load $R_{out}$ is occurred, where $I_{dc}$ means the output dc current. Fig. 12 (a) represents the periodical variation of the output reference voltage from 585 V to 650 V and Fig. 12 (b) shows the periodical change of the output load from 100 Ω to 50 Ω. From Fig. 12, it can be known that the proposed method can follow the output reference voltage with rapid dynamics in spite of the change of the output reference voltage and the output load.

Comparative results for the MPCC and the MPVFC methods according to the intensity of the harmonic distortion in the input voltage sources are shown in Figs 13 and 14. The average THD depicted in Figs 13, 14, 15, 16, and 17 is the average value of the three THD values obtained by the rectifier input current of phase $x$, calculated using (17).

$$THD_x(\%) = \frac{\sqrt{i_{conx}^2 - i_{conx1}^2}}{i_{conx1}} \times 100, \tag{17}$$

where, $i_{conx}$ $(x = a, b, c)$ is the rectifier input current of phase $x$ and $i_{conx1}$ is the fundamental component of the rectifier input current in phase $x$.

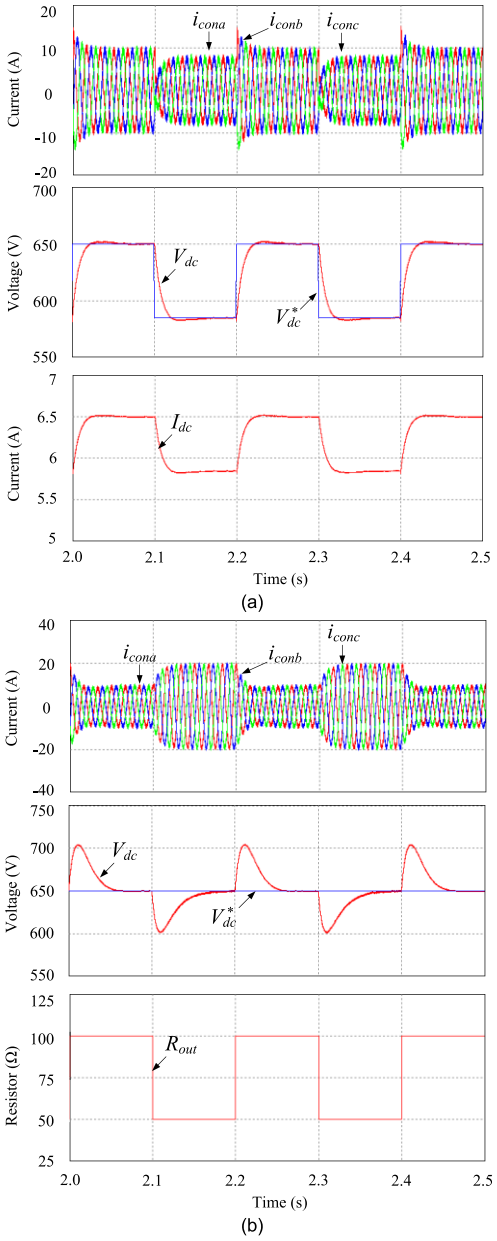


**FIGURE 12.** Simulation results when the periodical change of (a) the output reference voltage and (b) the output load is occurred.

Fig. 13 shows comparative results of the MPCC and MPVFC methods according to the intensity of distortion when the *a*-phase input voltage contains fifth harmonic components, as written in (16). It can be seen from Fig. 13 that the average THD values of the rectifier input currents obtained with the conventional MPCC method increase proportionally with the distortion in the *a*-phase input voltage. However, the average THD values of the rectifier input currents obtained with the proposed MPVFC method remain almost constant despite the increasing intensity of the distortion in the *a*-phase input voltage, as shown in Fig. 13.

Performance comparisons of the MPCC and the MPVFC methods depending on the distortion of the three-phase input

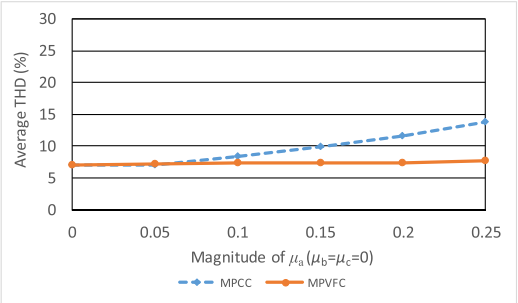


**FIGURE 13.** Average THD values of the rectifier input currents for the conventional MPCC method and the proposed MPVFC method according to the intensity of the distortion with fifth harmonics in *a*-phase of the input voltage.

voltages with fifth harmonic components as expressed in (16) are represented in Fig. 14. As shown in the figure, the average THD values of the rectifier input currents resulting from the conventional MPCC method sharply increase with distortion in the three-phase input voltages, whereas the dependency of the rectifier input current THD values on the three-phase input voltage distortion when using the proposed MPVFC method is much lower than for the conventional MPCC method.

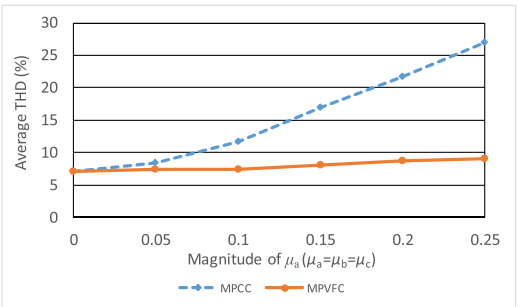


**FIGURE 14.** Average THD values of the rectifier input currents for the conventional MPCC method and the proposed MPVFC method depending on the intensity of the distortion with fifth harmonics in the three-phase input voltage.

Because the proposed MPVFC method utilizes model parameter values for practical rectifier elements, the robustness against the uncertainty between real and model parameter values is important. Therefore, in the case that there exist uncertainties in the line resistance and the line inductance in the AFE rectifier, the average THD values of the rectifier input currents obtained by the proposed MPVFC method were investigated along with those obtained with the conventional MPCC method for comparison purposes. Fig. 15 shows comparisons of the current errors and the average THD values of the rectifier input currents obtained using the MPCC and the MPVFC methods, in the case of no distortion of input voltages, according to the uncertainties of the line inductance and the line resistance. The current errors in the paper are calculated by (18). From Fig. 15, it can be seen that the dependency of the current errors and the average THD values

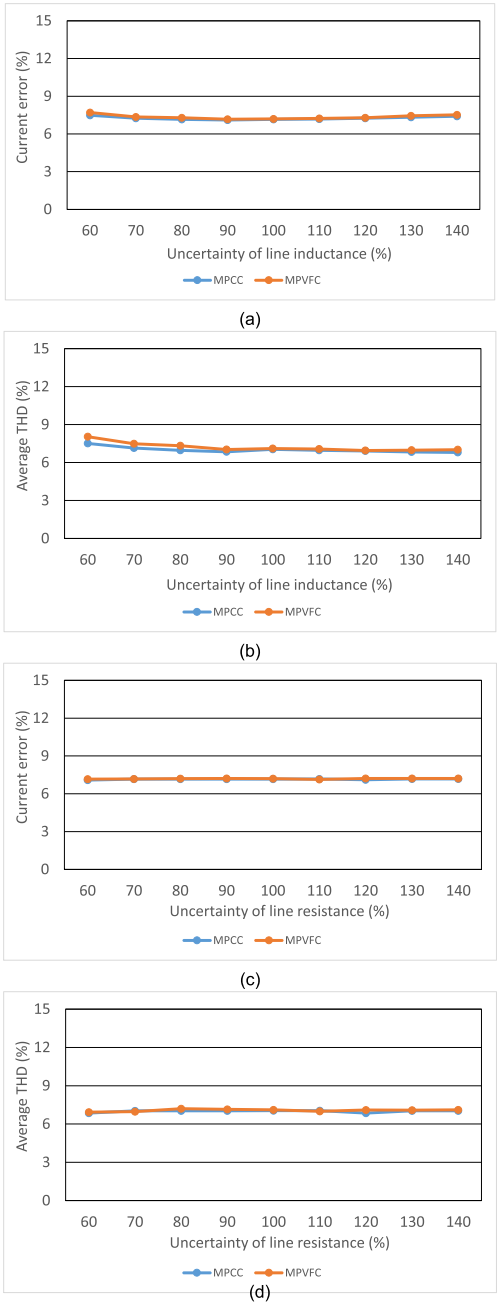


**FIGURE 15.** Comparisons of MPCC and MPVFC methods, in the case of no distortion of the input voltages (a) current errors according to the uncertainty of line inductance (b) average THD values according to the uncertainty of line inductance (c) current errors according to the uncertainty of line resistance (b) average THD values according to the uncertainty of line resistance.

on the line inductance and line resistance errors is almost same for both methods for a non-distorted input voltage.

$$\text{current error}\,(\%) = \frac{1}{2N}\Big(\sum_{k=1}^{N}\frac{\left|i^*_{con\alpha}(k) - i_{con\alpha}(k)\right|}{rms(i^*_{con\alpha}(k))} + \sum_{k=1}^{N}\frac{\left|i^*_{con\beta}(k) - i_{con\beta}(k)\right|}{rms(i^*_{con\beta}(k))}\Big) \times 100 \tag{18}$$

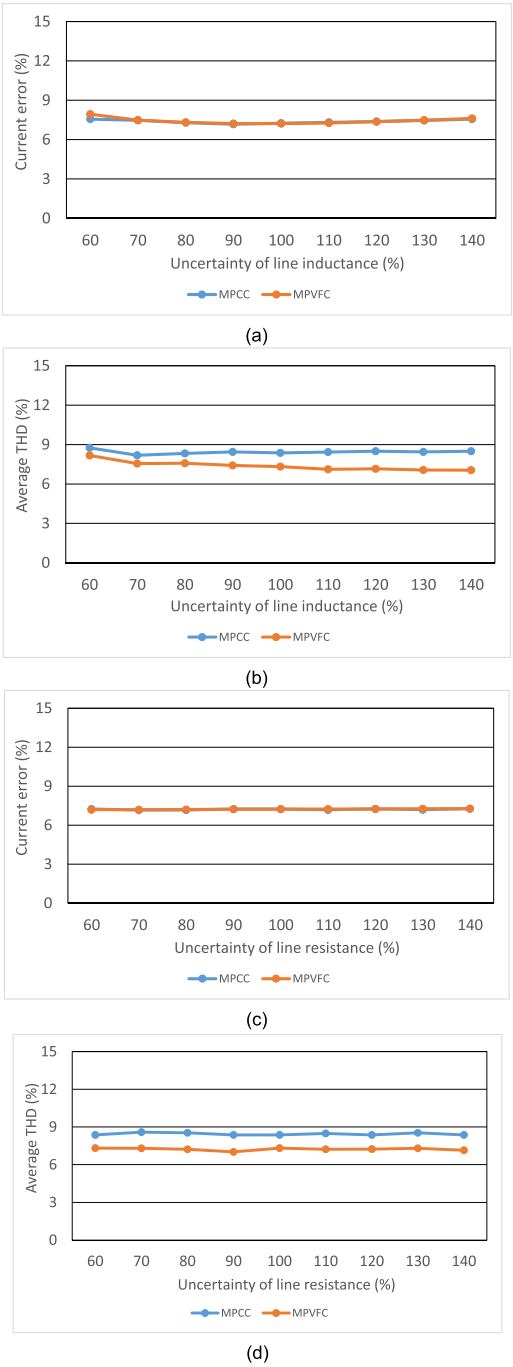


**FIGURE 16.** Comparisons of MPCC and MPVFC methods, in the case of distortion of the $a$-phase input voltage with $\mu_a = 0.1$ and $\mu_b = \mu_c = 0$, (a) current errors according to the uncertainty of line inductance (b) average THD values according to the uncertainty of line inductance (c) current errors according to the uncertainty of line resistance (b) average THD values according to the uncertainty of line resistance.

Fig. 16 shows comparisons of the current errors and the average THD values of the rectifier input currents obtained with the MPCC and the MPVFC methods, in the case of unbalanced distortion of the $a$-phase input voltage with $\mu_a = 0.1$ and $\mu_b = \mu_c = 0$, as expressed in (16), according to the uncertainties of the line inductance and the line resistance. In addition, Fig. 17 illustrates the current errors and the

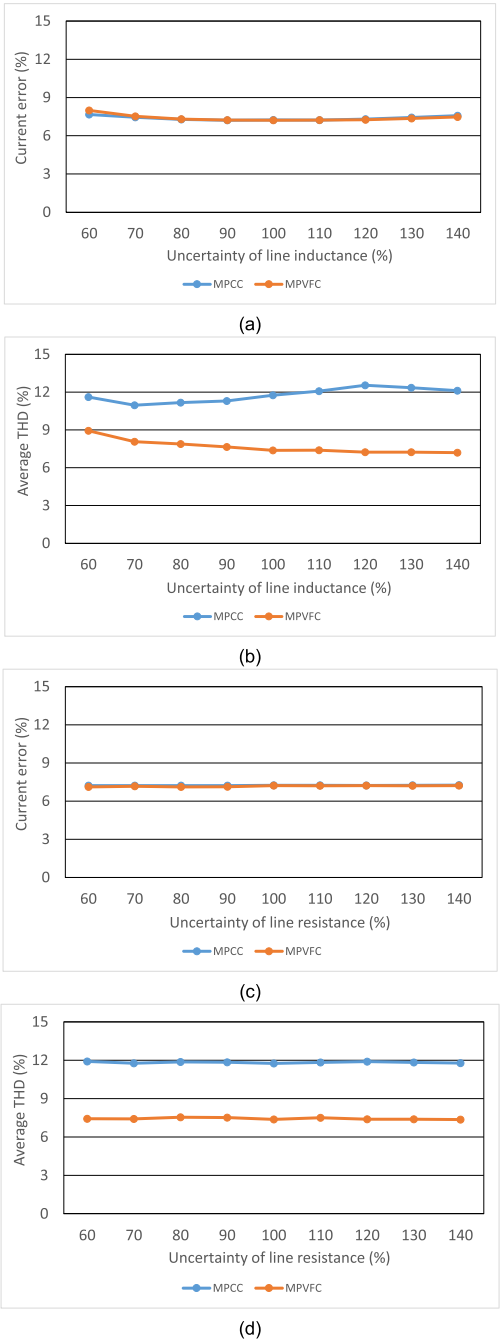


**FIGURE 17.** Comparisons of MPCC and MPVFC methods, in the case of distortion of the three-phase input voltage with $\mu_a = \mu_b = \mu_c = 0.1$, (a) current errors according to the uncertainty of line inductance (b) average THD values according to the uncertainty of line inductance (c) current errors according to the uncertainty of line resistance (b) average THD values according to the uncertainty of line resistance.

average THD values of the rectifier input currents obtained with both methods in the case of balanced distortion in the three-phase input voltage, with $\mu_a = \mu_b = \mu_c = 0.1$. In both figures, it can be known that the tendency of the current errors according to the uncertainty of the line inductance and the line resistance is almost equal to the case of Fig. 15. Also, the THD values obtained with the proposed method are lower

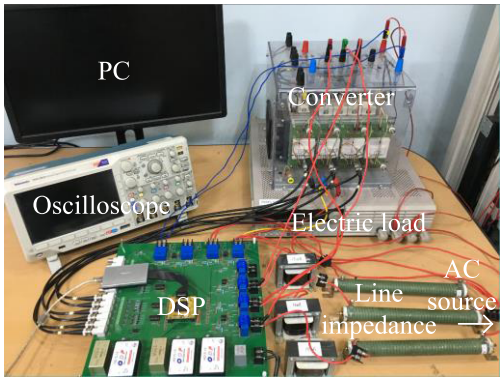


**FIGURE 18.** Experimental setup.

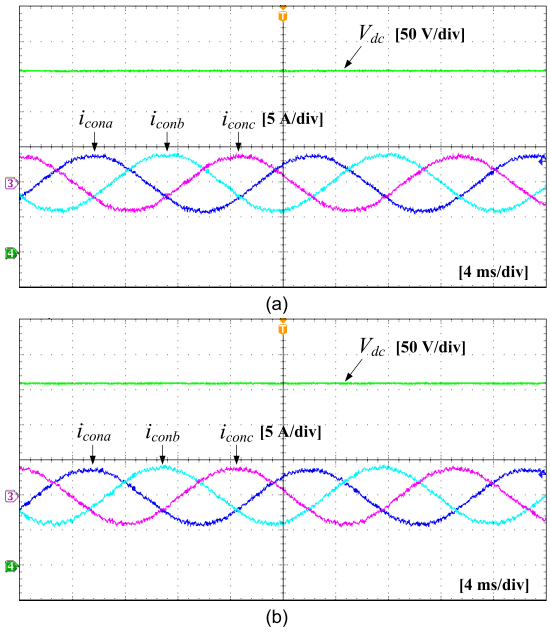


**FIGURE 19.** Experimental waveforms of the three-phase rectifier input currents and the output voltage with no input voltage distortion obtained with (a) the conventional MPCC method and (b) the proposed MPVFC method.

than those obtained with the conventional method with model errors in the line inductance and the line resistance. From Fig. 15, Fig. 16, and Fig. 17, the robustness of the proposed method against parameter uncertainty can be verified.

## V. EXPERIMENTAL RESULTS

Experiments were conducted to demonstrate the performance of the proposed MPVFC method based on the virtual flux. In these experiments, a prototype setup of a three-phase AFE rectifier composed of insulated-gate bipolar transistor (IGBT) modules (SKM50GB123D) with 1 Ω line resistors, 15 mH line inductors, a 1100 $\mu$F output capacitor, and a 100 Ω load resistance were used with a digital signal processor (DSP) board (TMS320F28335) as a controller, as shown in Fig. 18. In addition, an input voltage with a magnitude of 120 V and a fundamental frequency

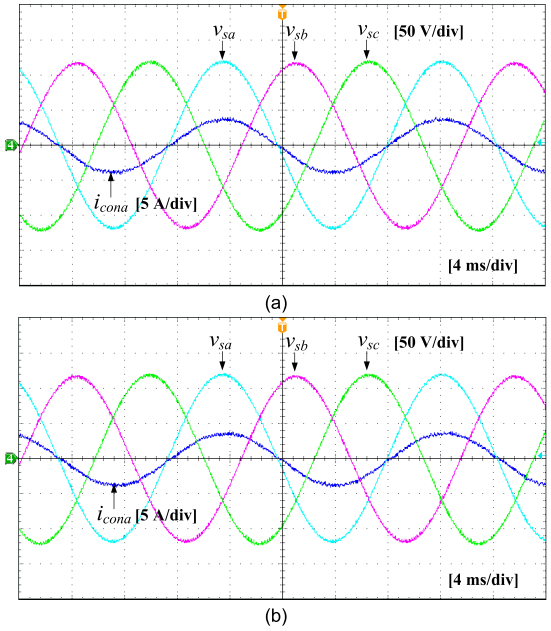


**FIGURE 20.** Experimental waveforms of the *a*-phase rectifier input current and the three-phase input voltage with no input voltage distortion obtained with (a) the conventional MPCC method and (b) the proposed MPVFC method.

of 60 Hz, a sampling period of 50 $\mu$s, and an output reference voltage of 260 V were used to control the AFE rectifier.

Figs. 19 and 20 show the experimental waveforms obtained with the conventional MPCC method and the proposed MPVFC method, in the case in which there existed no distortion in the input voltages. Fig. 19 illustrates the three-phase rectifier input currents and the output voltage; both methods yielded three-phase balanced sinusoidal waveforms with high quality as the input currents and the output voltage tracked its reference value under non-distorted input voltage conditions. Furthermore, the experimental waveforms of the *a*-phase rectifier input current and the three-phase input voltage generated by both methods are represented in Fig. 20. It can be noted that the two methods led to a sinusoidal input current that was in phase with the input voltage, yielding the unity power factor. As a result, there were no performance differences between the MPVFC method using the virtual fluxes as control variables and the MPCC method based on the input currents as control variables.

Fig. 21 represents the frequency spectrum of the *a*-phase input voltage, the *a*-phase rectifier input current obtained with the conventional MPCC method, and the *a*-phase rectifier input current obtained with the proposed MPVFC method for non-distorted input voltages. Because there was no distortion in the input voltage, the frequency spectrum of the input voltage only had the fundamental component, which is shown in Fig. 21 (a). From Figs. 21 (b) and (c), it can be seen that the frequency spectra of both methods are almost the same for non-distorted input voltages.

Figs. 22 and 23 depict the experimental results obtained with the conventional MPCC and the proposed

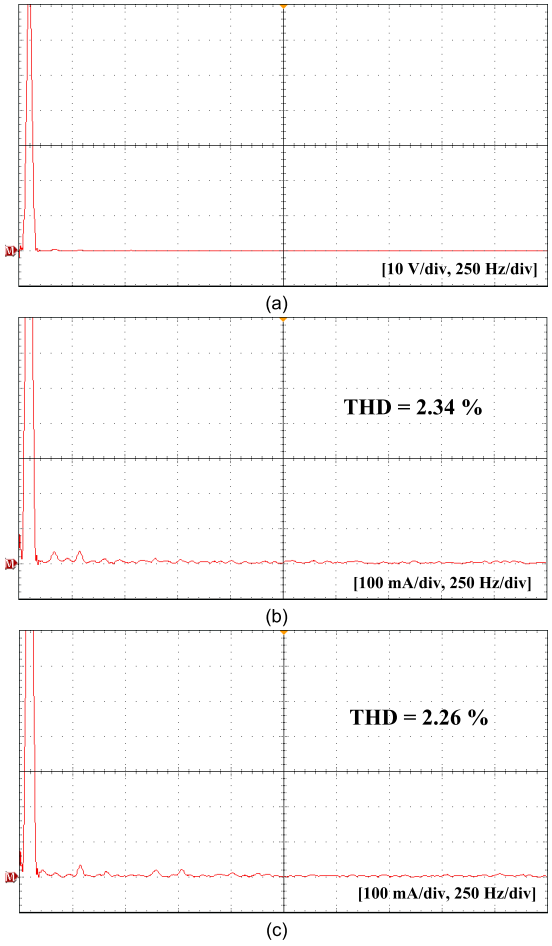


**FIGURE 21.** Frequency spectrum of the obtained experimental waveforms for non-distorted input voltages: (a) *a*-phase input voltage, (b) *a*-phase rectifier input current obtained with the conventional MPCC method, and (c) *a*-phase rectifier input current obtained with the proposed MPVFC method.

MPVFC methods, under unbalanced input voltage distortion conditions in which 10 % fifth harmonics were injected only to the *a*-phase input voltage, i.e., $\mu_a = 0.1$ and $\mu_b = \mu_c = 0$. It can be seen from Fig. 22 (a) that the conventional MPCC method yields distorted input current waveforms due to the input voltage distortion. On the other hand, the proposed MPVFC method generates three-phase rectifier input currents with sinusoidal waveforms with much less distortion than the conventional MPCC method, despite the input voltage contamination, thanks to the control structure based on the virtual fluxes. In addition, the *a*-phase rectifier input current and the three-phase input voltage waveforms generated by both methods under input voltage distortion conditions are illustrated in Fig. 23. The input current waveform obtained with the MPCC method, shown in Fig. 23 (a), is distorted with the fifth harmonic component, similarly to the distorted input voltage waveform. However, the proposed MPVFC method results in a sinusoidal input current waveform; thus, the input current quality obtained with the proposed method is less degraded by input voltage distortions than that obtained with the conventional MPCC method.

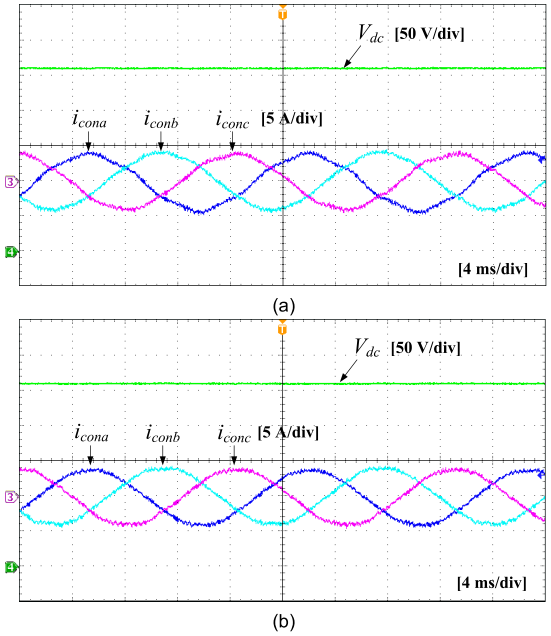


**FIGURE 22.** Experimental waveforms of the three-phase rectifier input currents and the output voltage with $a$-phase input voltage distortion ($\mu_a = 0.1$ and $\mu_b = \mu_c = 0$) obtained with (a) the conventional MPCC method and (b) the proposed MPVFC method.

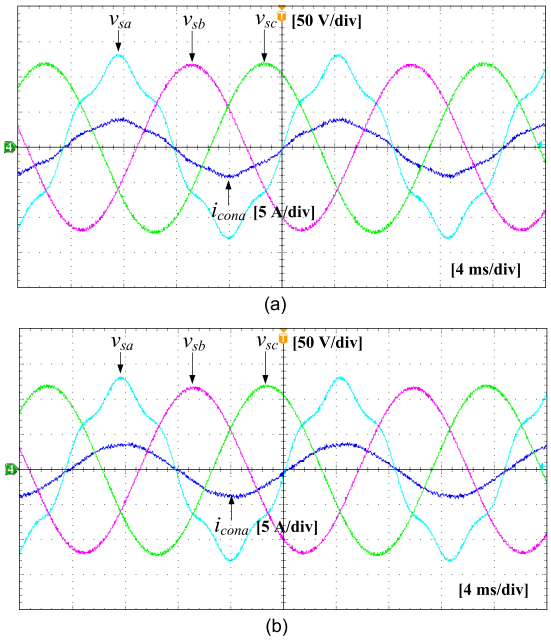


**FIGURE 23.** Experimental waveforms of the $a$-phase rectifier input current and the three-phase input voltage with $a$-phase input voltage distortion ($\mu_a = 0.1$ and $\mu_b = \mu_c = 0$)obtained with (a) the conventional MPCC method and (b) the proposed MPVFC method.

Fig. 24 illustrates the frequency spectra of the $a$-phase input voltage, the $a$-phase rectifier input current obtained with the conventional MPCC method, and the $a$-phase rectifier input current obtained with the proposed MPVFC method under 10 % fifth harmonic distortion conditions. As shown in Fig. 24 (a), under 10 % fifth harmonic distortion

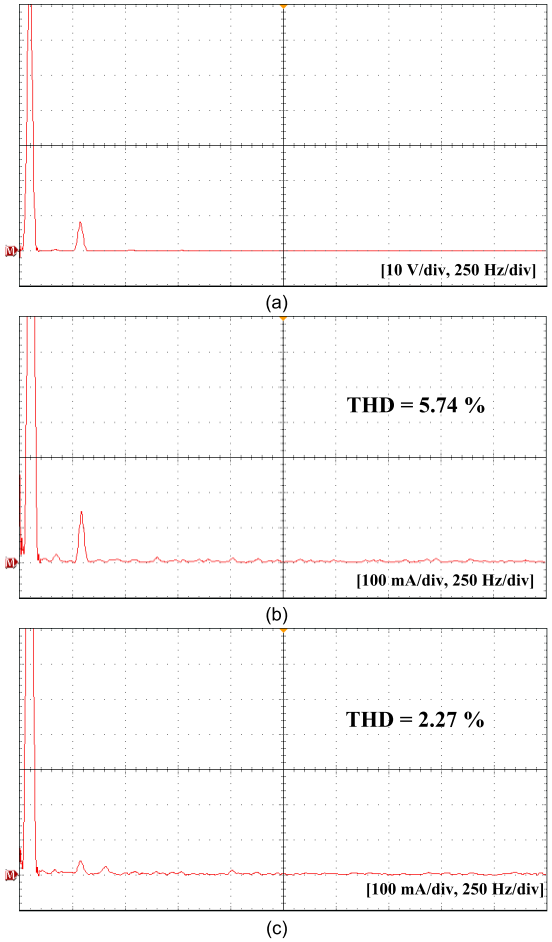


**FIGURE 24.** Frequency spectra of the experimental waveforms under 10 % fifth harmonic distortion conditions: (a) $a$-phase input voltage, (b) $a$-phase rectifier input current obtained with the conventional MPCC method, and (c) $a$-phase rectifier input current obtained with the proposed MPVFC.

conditions, the frequency spectrum of the $a$-phase input voltage contains the fifth harmonic component. Additionally, from Fig. 24 (b), it can be noted that the frequency spectrum of the $a$-phase rectifier input current obtained with the conventional MPCC method has the fifth harmonic component, which is not present in the case of a non-distorted input voltage. On the other hand, the frequency spectrum obtained with the proposed MPVFC method has a smaller fifth harmonic component than that of the conventional MPCC method thanks to its use of the virtual fluxes, which are resistant to harmonic distortion. From the results of the simulations and the experiments, it can be seen that the proposed MPVFC method can work well in various model parameters and diverse situations of the input voltage.

## VI. CONCLUSION

The MPVFC method utilizing the virtual fluxes as control variables is proposed to mitigate the performance degradation experienced by AFE rectifiers with distorted input voltages. The proposed MPVFC method controls the rectifier based on a control structure that uses the virtual fluxes, which are

resistant to input voltage distortions, whereas the conventional MPCC method directly uses the input voltages and currents to construct the cost function, which degrades its performance if there are input voltage distortions. The proposed model predictive control platform with the prediction and the cost function based on the rectifier virtual fluxes was developed to utilize the virtual fluxes as control variables. The effectiveness of the proposed MPVFC method was demonstrated by simulations and with our experimental results, in which input current waveforms with reduced distortion were achieved under input voltage distortion conditions.

## REFERENCES


[1] J. R. Rodriguez, J. W. Dixon, J. R. Espinoza, J. Pontt, and P. Lezana, "PWM regenerative rectifiers: State of the art," *IEEE Trans. Ind. Electron.*, vol. 52, no. 1, pp. 5–22, Feb. 2005.

[2] M. Kazmierkowski, R. Krishnan, and F. Blaabjerg, *Control in Power Electronics*. New York, NY, USA: Academic, 2002.

[3] T. Noguchi, H. Tomiki, S. Kondo, and I. Takahashi, "Direct power control of PWM converter without power-source voltage sensors," *IEEE Trans. Ind. Appl.*, vol. 34, no. 3, pp. 473–479, May 1998.

[4] S. Vazquez, J. A. Sanchez, J. M. Carrasco, J. I. Leon, and E. Galvan, "A model-based direct power control for three-phase power converters," *IEEE Trans. Ind. Electron.*, vol. 55, no. 4, pp. 1647–1657, Apr. 2008.

[5] M. Malinowski, M. Jasinski, and M. P. Kazmierkowski, "Simple direct power control of three-phase PWM rectifier using space-vector modulation (DPC-SVM)," *IEEE Trans. Ind. Electron.*, vol. 51, no. 2, pp. 447–454, Apr. 2004.

[6] A. Bouafia, J. P. Gaubert, and F. Krim, "Predictive direct power control of three-phase pulsewidth modulation (PWM) rectifier using space-vector modulation (SVM)," *IEEE Trans. Power Electron.*, vol. 25, no. 1, pp. 228–236, Jan. 2010.

[7] C. Lascu, I. Boldea, and F. Blaabjerg, "A modified direct torque control for induction motor sensorless drive," *IEEE Trans. Ind. Appl.*, vol. 36, no. 1, pp. 122–130, Jan. 2000.

[8] A. Bouafia, F. Krim, and J. P. Gaubert, "Fuzzy-logic-based switching state selection for direct power control of three-phase PWM rectifier," *IEEE Trans. Ind. Electron.*, vol. 56, no. 6, pp. 1984–1992, Jun. 2009.

[9] J. Hu, L. Shang, Y. He, and Z. Q. Zhu, "Direct active and reactive power regulation of grid-connected DC/AC converters using sliding mode control approach," *IEEE Trans. Power Electron.*, vol. 26, no. 1, pp. 210–222, Jan. 2011.

[10] M. Malinowski, M. P. Kazmierkowski, and A. M. Trzynadlowski, "A comparative study of control techniques for PWM rectifiers in AC adjustable speed drives," *IEEE Trans. Power Electron.*, vol. 18, no. 6, pp. 1390–1396, Nov. 2003.

[11] M. Malinowski, M. P. Kazmierkowski, S. Hansen, F. Blaabjerg, and G. D. Marques, "Virtual-flux-based direct power control of three-phase PWM rectifiers," *IEEE Trans. Ind. Appl.*, vol. 37, no. 4, pp. 1019–1027, Jul./Aug. 2001.

[12] Y. Cho and K.-B. Lee, "Virtual-flux-based predictive direct power control of three-phase PWM rectifiers with fast dynamic response," *IEEE Trans. Power Electron.*, vol. 31, no. 4, pp. 3348–3359, Apr. 2016.

[13] J. Rodríguez *et al.*, "State of the art of finite control set model predictive control in power electronics," *IEEE Trans. Ind. Informat.*, vol. 9, no. 2, pp. 1003–1016, May 2013.

[14] I. S. Mohamed, S. A. Zaid, M. F. Abu-Elyazeed, and H. M. Elsayed, "Implementation of model predictive control for three-phase inverter with output LC filter on eZdsp F28335 Kit using HIL simulation," *Int. J. Model., Identificat. Control*, vol. 25, no. 4, pp. 301–312, 2016.

[15] S. Kwak and J.-C. Park, "Predictive control method with future zero-sequence voltage to reduce switching losses in three-phase voltage source inverters," *IEEE Trans. Power Electron.*, vol. 30, no. 3, pp. 1558–1566, Mar. 2015.

[16] J. Rodríguez *et al.*, "Predictive current control of a voltage source inverter," *IEEE Trans. Ind. Electron.*, vol. 54, no. 1, pp. 495–503, Feb. 2007.

[17] P. Cortes, J. Rodriguez, C. Silva, and A. Flores, "Delay compensation in model predictive current control of a three-phase inverter," *IEEE Trans. Ind. Electron.*, vol. 59, no. 2, pp. 1323–1325, Feb. 2012.

[18] J. Rodriguez and P. Cortes, *Predictive Control of Power Converters and Electrical Drives*. New York, NY, USA: Wiley, 2012, pp. 31–39.

[19] D.-K. Choi and K.-B. Lee, "Dynamic performance improvement of AC/DC converter using model predictive direct power control with finite control set," *IEEE Trans. Ind. Electron.*, vol. 62, no. 2, pp. 757–767, Feb. 2015.

[20] S. Kwak and J. C. Park, "Model-predictive direct power control with vector preselection technique for highly efficient active rectifiers," *IEEE Trans. Ind. Informat.*, vol. 11, no. 1, pp. 44–52, Feb. 2015.

[21] M. Parvez, S. Mekhilef, N. M. L. Tan, and H. Akagi, "An improved active-front-end rectifier using model predictive control," in *Proc. IEEE Appl. Power Electron. Conf. Expo. (APEC)*, Mar. 2015, pp. 122–127.

[22] I. S. Mohamed, S. A. Zaid, M. F. Abu-Elyazeed, and H. M. Elsayed, "Improved model predictive control for three-phase inverter with output LC filter," *Int. J. Model., Identificat. Control*, vol. 23, no. 4, pp. 371–379, 2015.

[23] I. S. Mohamed, S. A. Zaid, M. F. Abu-Elyazeed, and H. M. Elsayed, "Model predictive control-a simple and powerful method to control UPS inverter applications with output LC filter," in *Proc. Saudi Int. Electron., Commun. Photon. Conf.*, 2013, pp. 1–6.

[24] P. Antoniewicz and M. P. Kazmierkowski, "Virtual-flux-based predictive direct power control of AC/DC converters with online inductance estimation," *IEEE Trans. Ind. Electron.*, vol. 55, no. 12, pp. 4381–4390, Dec. 2008.

[25] M. H. Saeedinia and S. A. Davari, "Virtual flux model predictive direct power control (VF-MPDPC) of AFE rectifier with new current prediction method and negative sequence elimination," in *Proc. IEEE Int. Symp. PRECEDE*, Sep. 2017, pp. 113–118.

[26] M. P. Akter, S. Mekhilef, N. M. L. Tan, and H. Akagi, "Modified model predictive control of a bidirectional AC–DC converter based on Lyapunov function for energy storage systems," *IEEE Trans. Ind. Electron.*, vol. 63, no. 2, pp. 704–715, Feb. 2016.

[27] M. P. Akter, S. Mekhilef, N. M. L. Tan, and H. Akagi, "Stability and performance investigations of model predictive controlled active-front-end (AFE) rectifiers for energy storage systems," *J. Power Electron.*, vol. 15, pp. 202–215, Feb. 2015.

[28] U. Muslem, S. Mekhilef, M. Rivera, and J. Rodriguez, "Imposed weighting factor optimization method for torque ripple reduction of IM fed by indirect matrix converter with predictive control algorithm," *J. Elect. Eng. Technol.*, vol. 10, no. 1, pp. 227–242, 2015.

[29] M. P. Akter, S. Mekhilef, N. M. L. Tan, and H. Akagi, "Model predictive control of bidirectional AC–DC converter for energy storage system," *J. Elect. Eng. Technol.*, vol. 10, no. 1, pp. 165–175, 2015.

[30] J. L. Duarte, A. V. Zwam, C. Wijnands, and A. Vandenput, "Reference frames fit for controlling PWM rectifiers," *IEEE Trans. Ind. Electron.*, vol. 46, no. 3, pp. 628–630, Jun. 1999.


**JAE-CHANG KIM** received the B.S. degree in electrical and electronics engineering from Chung-Ang University, Seoul, South Korea, in 2017. He is currently pursuing the M.S and Ph.D. combined degree in electrical and electronics engineering with Chung-Ang University. His research interests are control and analysis for two-level, multilevel, and matrix converters.

**SANGSHIN KWAK** (S'02–M'05) received the Ph.D. degree in electrical engineering from Texas A&M University, College Station, TX, USA, in 2005. From 1999 to 2000, he was a Research Engineer with LG Electronics, Changwon, South Korea. He was also with Whirlpool R&D Center, Benton Harbor, MI, USA, in 2004. From 2005 to 2007, he was a Senior Engineer with Samsung SDI R&D Center, Yongin, South Korea. From 2007 to 2010, he was an Assistant Professor with Daegu University, Gyeongsan, South Korea. Since 2010, he has been with Chung-Ang University, Seoul, South Korea, where he is currently a Professor. His research interests are topology design, modeling, modulation, and control of power converters, multilevel converters, renewable energy systems, and power quality.